ELSEVIER

International Journal of Heat and Fluid Flow 19 (1998) 233–244

International Journal of HEAT AND FLUID FLOW

Heat transfer and velocity fluctuations in a staggered tube array

J.W. Scholten [1], D.B. Murray *

Department of Mechanical Engineering, Trinity College, Dublin 2, Ireland

Received 9 January 1997; accepted 20 October 1997

Abstract

This paper describes an experimental investigation of unsteady heat transfer and velocity in a staggered tube array. The velocity measurements were obtained with a laser Doppler anemometer and a surface mounted hot film sensor was used to make the heat flux measurements. Data are presented in the form of time-averaged Nusselt numbers and fluctuating heat transfer rates, along with velocity and heat flux autospectra. The coherence and phase difference between the velocity and heat flux signals is included also. For the front of a cylinder in the first row, the results obtained indicate that the fluctuations in surface heat flux originate in whole field velocity pulsation resulting from vortex shedding. For the remainder of the array, the results indicate that the heat flux variation is governed by turbulent eddy transport originating in the breakdown of shed vortices as the flow progresses through the array.

Keywords: Unsteady heat transfer; Hot film sensor; Laser Doppler anemometer; Simultaneous velocity and heat flux measurements; Staggered tube array

Notation

A_{eff}	effective surface area of the hot film sensor
D	diameter of the test cylinder
k_{kapton}	conductivity of kapton substrate
k_{air}	conductivity of air
Nu	Nusselt number
q_{cond}	conductive heat flux through substrate
q_{conv}	convective heat flux
Q_{diss}	electrically dissipated power in the sensor
R_{arm}	electrical resistance of the active bridge arm
R_{sensor}	electrical resistance of the sensor
R_{top}	top resistance in the bridge
T_{amb}	ambient temperature
T_{sensor}	sensor temperature
T_{tube}	tube temperature
$T_{\text{tube, 0}}$	tube temperature at zero flow velocity
V_{bridge}	bridge voltage
V_0	bridge voltage at zero flow velocity
δ	thickness of the sensor substrate

1. Introduction

Studies of heat transfer from tube arrays in cross flow have been widely reported. For example, Zukauskas (1972) reviewed the local heat transfer performance of tube arrays in cross flow and Achenbach (1981) investigated the local heat transfer characteristics of both in-line and staggered tube banks. The results of these studies are, however, limited to time averaged local and mean Nusselt numbers whereas time resolved heat transfer information is more useful for the identification of convective heat transfer mechanisms.

Measurements of unsteady heat transfer from cylinders in cross flow are more difficult to obtain, due to the high frequency and small amplitude of the random fluctuations encountered. Fluctuations in heat transfer for an oscillating cylinder in cross flow were measured by Rosicskowski and Hollworth (1991), but this study was limited to the low frequencies associated with the cylinder oscillations. Likewise, for cylinders immersed in gas fluidised beds, the studies of George (1993), Katoh et al. (1991) and Rottger and Renz (1994) have all investigated the instantaneous local heat transfer characteristics. Again, the frequencies associated with bubble motion and particle contact at the tube surface are much lower than encountered in turbulent cross flows. For a cylinder in a cross flow of high turbulence intensity, Simmons et al. (1990) and Ching and O'Brien (1991) have recorded fluctuations in the heat transfer rates from measurements at the front stagnation point. Fluctuating heat transfer at different angular positions on the surface of a single cylinder in cross flow has been investigated by Scholten and Murray (1995) and limited data for a cylinder located within a cluster of three cylinders were reported by Scholten et al. (1996a, b).

* Corresponding author.

[1] Currently at Laboratoire d'Acoustique de l'Université du Maine, URA, 1101 Avenue O.Messiaen, BP535, 72017 le Mans Cedex, France.

0142-727X/98/$19.00
PII: S0142-727X(98)00007-1

The fluctuating flow field around cylinders in cross flow has also been investigated. For example, Meyer and Larsen (1994) and Balabani and Yianneskis (1996) used laser Doppler anemometry to investigate the mean flow and turbulence structure for flows through tube arrays. However, for the identification of convective heat transfer mechanisms in highly turbulent flows, such as encountered in tube arrays, simultaneous measurement of fluctuating heat flux and velocity signals is needed to enable the link between local flow structure and surface heat transfer to be determined.

This paper describes simultaneous measurements of surface heat flux and velocity close to the surface of a tube located within a small staggered array of tubes. Tests were conducted for two Reynolds numbers and three tube locations, with results presented in the form of heat flux and velocity autospectra together with the coherence and phase difference between the heat flux and velocity signals. In addition, local time-averaged Nusselt numbers are reported.

2. Experimental set-up

The test facilities consist of a low turbulence (≅0.5%) wind tunnel with a perspex test section 127 mm square and 500 mm in length. A 60° triangular tube array of 3 rows with tube pitch to diameter ratio of 2 was installed horizontally in this test section. The measurements were obtained from the central tube in the row of 3, thereby reducing the influence of the tunnel wall. Details of the tube array geometry used for first, second and third row testing are given in Fig. 1. Aluminium tubes of 25 mm diameter were used in conjunction with a single instrumented tube which was constructed from thick walled copper with an internal cartridge heater, approximating a uniform wall temperature boundary condition. The ends of the tube were constructed of tufnol to reduce axial heat loss. Midway along the tube length, a thin constantan wire was embedded flush with the surface, and the tip of the wire was electrically connected to the copper of the tube to form a type T thermocouple junction. A Dantec 55R47 hot film sensor was mounted directly above this thermocouple junction in such a way that the hot film itself was aligned with the axis of the cylinder, giving a circumferential resolution of 0.9°. In order to obtain data for different positions on the tube circumference, the tube was rotated at 5° intervals. All leads were brought out of the test section through one of the tufnol end pieces. The hot film was connected to a Dantec 55M10 standard bridge, which maintained the temperature of the hot film at a specified value. Both the hot film and the surface thermocouple were calibrated against a reference thermometer, giving absolute uncertainties in temperature of ±0.3°C. However, the uncertainty in temperature difference between the hot film and the tube surface is ±0.1°C. The 90% frequency response for the hot film was found to be about 10 kHz by using a square wave test.

Laser Doppler anemometry was used for the velocity measurements close to the heated tube surface. The laser Doppler system consisted of a 32 mW HeNe laser with Bragg cell for frequency shifting, and was used in the forward scatter mode. The photomultiplier signal was processed by a TSI 1980B counter type processor which outputs velocity data points together with the time between successive data points.

2.1. Data acquisition and processing

The output from the bridge and the output from the embedded thermocouple junction were logged on a Pentium P5-60

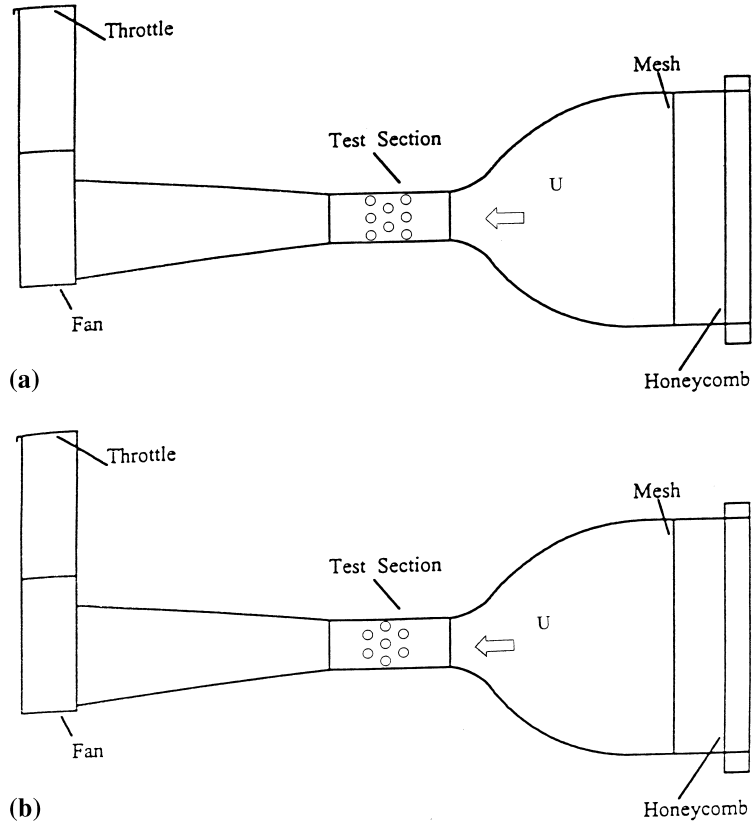

Fig. 1. Tube array configuration in wind tunnel testing: first and third rows (a), second row (b).

computer through 2 channels of an Amplicon PC-30PGL AtoD board. The heat flux values were then calculated by dividing the electrical power dissipated in the hot film sensor (determined from the Wheatstone bridge/sensor set-up)

$$Q_{\text{diss}} = (V_{\text{bridge}}^2 - V_0^2)\frac{R_{\text{sensor}}}{(R_{\text{arm}} + R_{\text{top}})^2} \quad (1)$$

by the effective surface area of the sensor (Beasley and Figliola, 1988), giving

$$q_{\text{diss}} = \frac{Q_{\text{diss}}}{A_{\text{eff}}}. \quad (2)$$

The main contribution of conduction to the tube through the sensor substrate is in the power dissipation associated with voltage V_0, which corresponds to the no flow condition. However, as the tube temperature under test conditions may differ slightly from that with zero flow, additional conduction between the sensor and tube is accounted for by use of the embedded thermocouple:

$$q_{\text{cond}} = k_{\text{kapton}}\frac{T_{\text{tube}} - T_{\text{hotfilm}}}{\delta} - k_{\text{kapton}}\frac{T_{\text{tube},0} - T_{\text{hotfilm}}}{\delta}. \quad (3)$$

This conduction correction term is minimised by careful control of the tube temperature and rarely exceeds 5–10% of the power dissipated in the hot film sensor. The total convective heat flux is then given by

$$q_{\text{conv}} = q_{\text{diss}} + q_{\text{cond}} \quad (4)$$

in which the positive sign results from the definition used for the additional conduction term. The convective heat flux is then non-dimensionalised to give the Nusselt number as

$$\text{Nu} = \frac{q_{\text{conv}}D}{k_{\text{air}}(T_{\text{sensor}} - T_{\text{amb}})}. \quad (5)$$

Data acquisition for the combination of LDA and heat transfer rates was performed by simultaneous recording through the direct memory access technique (DMA) into the computer, and *A–D* conversions were started by a triggering pulse from the LDA-counter processor in such a way that a heat transfer data point is taken each time an LDA point is taken. The velocity and heat flux data, which both consist of discrete data points and time-between-data points, were resampled at equidistant time intervals by using a 1st order interpolation. This has been shown by Simon et al. (1995) to reduce bias in spectral estimates from randomly sampled data.

The degree of correlation between turbulence and heat flux was estimated using coherence functions which give the degree of correlation as a function of frequency and are considered to provide the most insight into the underlying mechanisms of turbulent heat transfer. The auto spectra for the turbulence and heat transfer data were calculated using FFT based procedures and the coherence function, which is a normalised form of the cross spectrum (Bendat and Piersol, 1986), was computed from these. In addition, the phase difference between velocity and heat flux signals provides information on the influence of the flow structure on fluctuating heat transfer.

2.2. Experimental uncertainty

The effective surface area is the surface area modified to take account of lateral conduction and is estimated by calibration of the Nusselt number values, i.e. the surface area is adjusted until the Nusselt numbers obtained from calibration measurements match relevant Nusselt numbers from the literature. Although the resulting effective surface area is within the range quoted by Beasley and Figliola (1988), this calibration process represents the main source of uncertainty in the estimate of Nusselt number. The measured Nusselt numbers are repeatable to within ±2% but the systematic error associated with estimation of the effective surface area may be as high as 15%.

3. Results

3.1. First row

Fig. 2 shows the time-averaged local Nusselt numbers, obtained from hot film data, for a first row cylinder with upstream velocities of 5 and 15 m/s. This corresponds to array Reynolds numbers of 20 000 and 60 000 respectively (based on the tube diameter and the maximum gap velocity within the array). At 5 m/s, the variation in heat transfer around the tube is similar to that for a single cylinder in cross flow, with the minimum at 100° corresponding to boundary layer separation. This late boundary layer separation for the tube

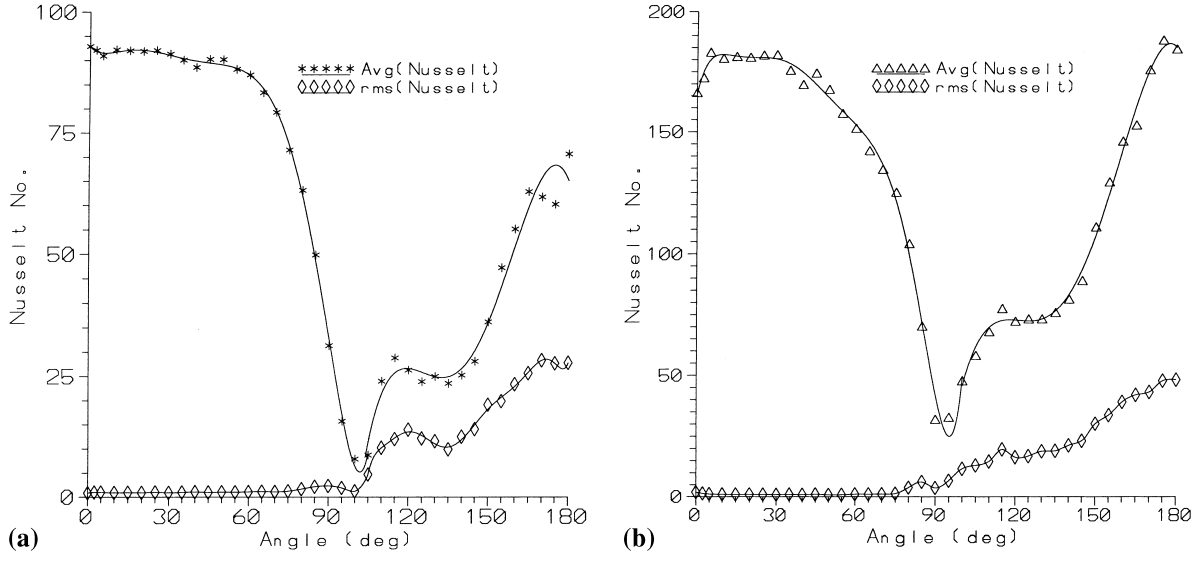

Fig. 2. Local Nusselt numbers at the first row: (a) $U = 5$ m/s; (b) $U = 15$ m/s.

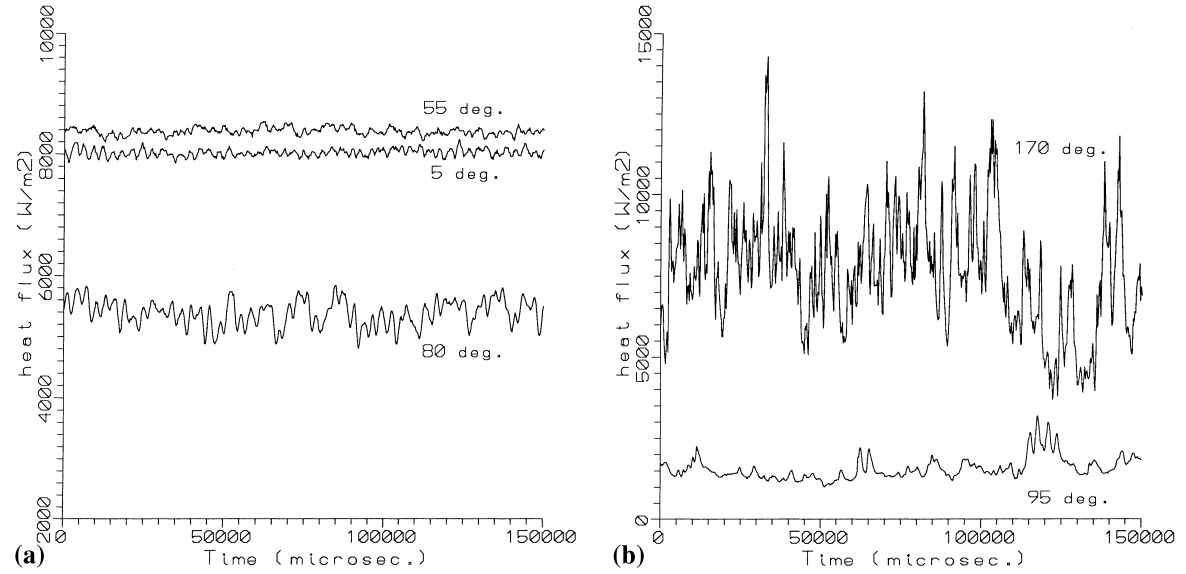

Fig. 3. Heat transfer time traces at the first row: $U = 15$ m/s: (a) positions preceding separation; (b) positions following separation.

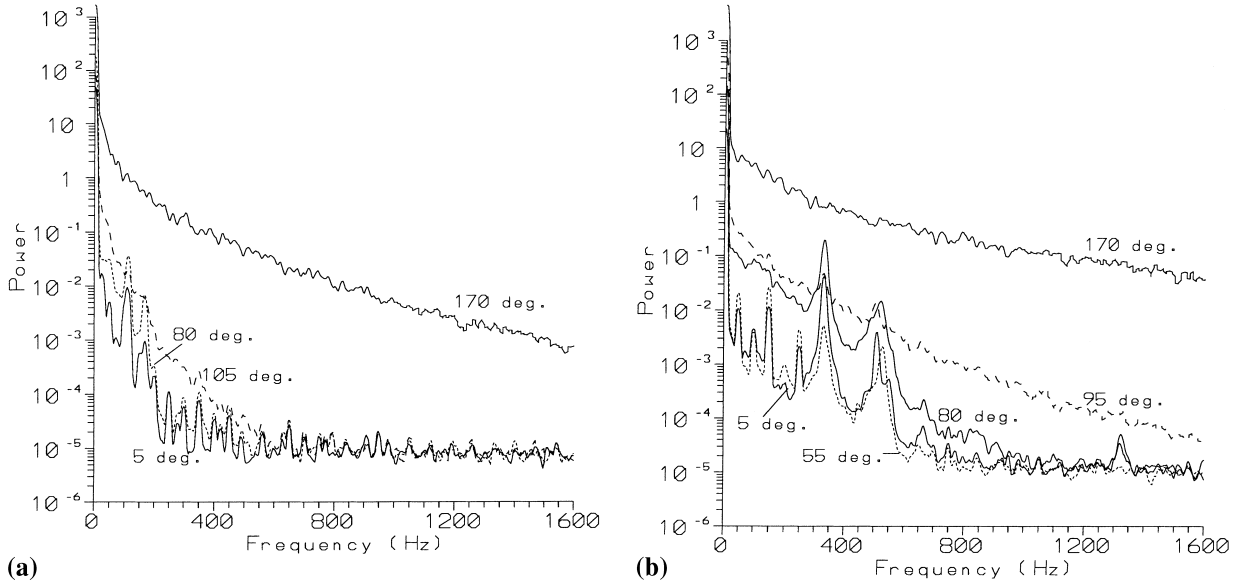

Fig. 4. Heat transfer auto spectra at the first row: (a) $U = 5$ m/s; (b) $U = 15$ m/s.

in the first row, as compared with a single cylinder in cross flow, is a consequence of blockage effects, as described by Baughn et al. (1986). Increasing the velocity to 15 m/s leads to higher Nusselt numbers together with earlier boundary layer separation, as indicated by the minimum Nusselt number at 90°/95°. The mean Nusselt number is higher, by 4% in the case of the lower velocity and by 17% for the higher velocity, than the value calculated from the correlation of Churchill and Bernstein (1977) for a single cylinder in cross flow. Again, this can be attributed to blockage effects and acceleration. In addition to the time-averaged Nusselt numbers, the rms values of the unsteady heat transfer are shown. It can be seen that the fluctuations at the front of the cylinder are extremely small, whereas the fluctuations over the rear of the cylinder are large due to extensive mixing and recirculation in the wake.

In Fig. 3, time traces of the heat flux signal for a number of angular positions on the cylinder surface are shown for the velocity of 15 m/s. For positions preceding boundary layer separation, a strong periodicity can be seen. For positions following separation, there is a higher content of random fluctuations with less evidence of periodicity. Fig. 4 shows the auto spectra of the heat transfer rate at the first row for locations

Table 1
Expected vortex shedding frequencies at first row (Zukauskas and Katinas, 1980) and second row (Weaver et al., 1987)

Velocity (m/s)	First row		Second row	
	Frequency (Hz)	Strouhal number	Frequency (Hz)	Strouhal number
5	168	0.84	115	0.58
15	504	0.84	347	0.58

in advance of and following boundary layer separation. Because of the high noise content in the signal at the lower velocity, it is difficult to identify dominant peaks in the frequency spectrum. However, peaks are present at 110 and 170 Hz. From Table 1, which summarises the expected vortex shedding frequencies for first row tubes from Zukauskas and Katinas (1980) and for second row tubes from Weaver et al. (1987), it is evident that these peaks correspond to vortex shedding from the second and first rows, respectively. It appears that vortex shedding from the second row causes a pulsating blockage effect which influences heat transfer at the first row. For the higher velocity, several frequency peaks can be seen with the dominant peaks at 325 and 515 Hz corresponding to vortex shedding from the second and first rows, respectively. The other sharp peaks that can be seen in the spectra result from 50 Hz mains noise and associated harmonics. An additional small peak at around 1325 Hz is evident on the traces for 5° and 80°; the origin of this high frequency is not clear. Although the frequency peaks associated with vortex shedding can still be detected after separation, it is clear that the level of high frequency fluctuations is increased significantly.

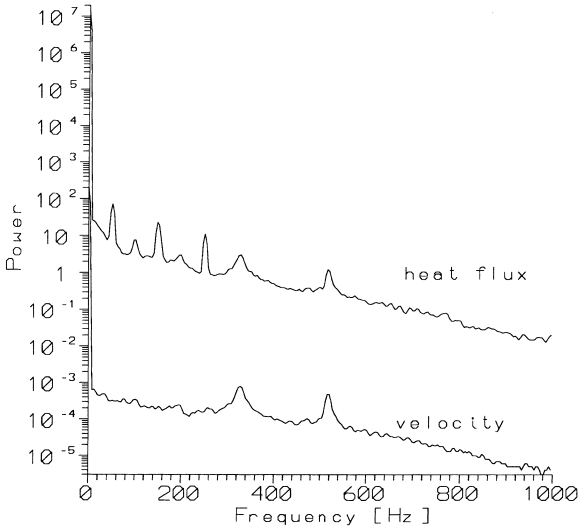

Fig. 5. Simultaneous auto spectra at the first row, 65°.

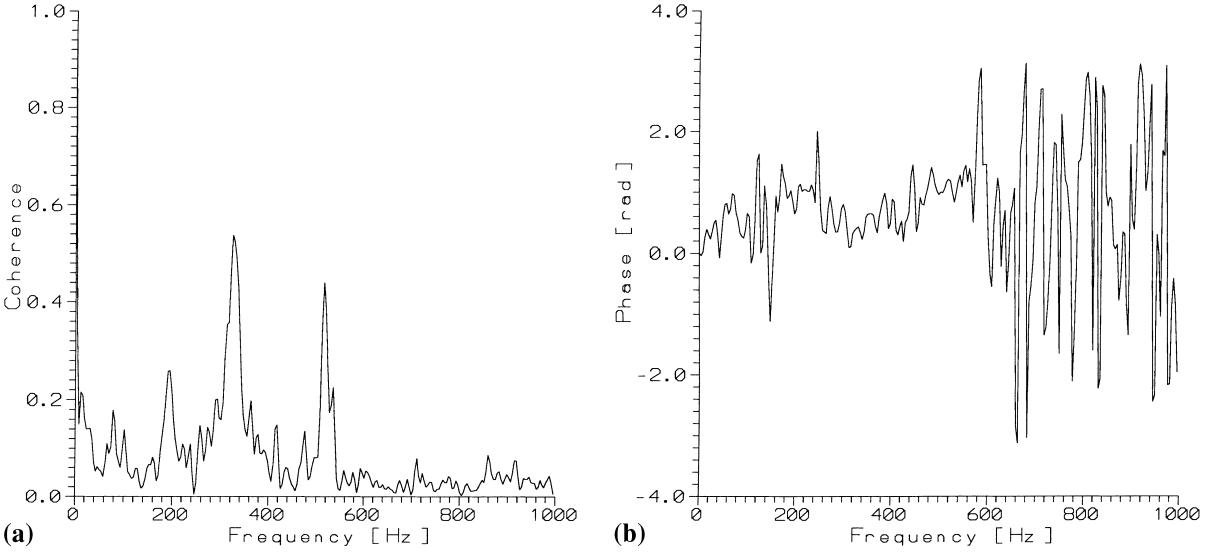

Fig. 6. Coherence and phase difference of LDA and heat flux signals at the first row: (a) coherence; (b) phase difference.

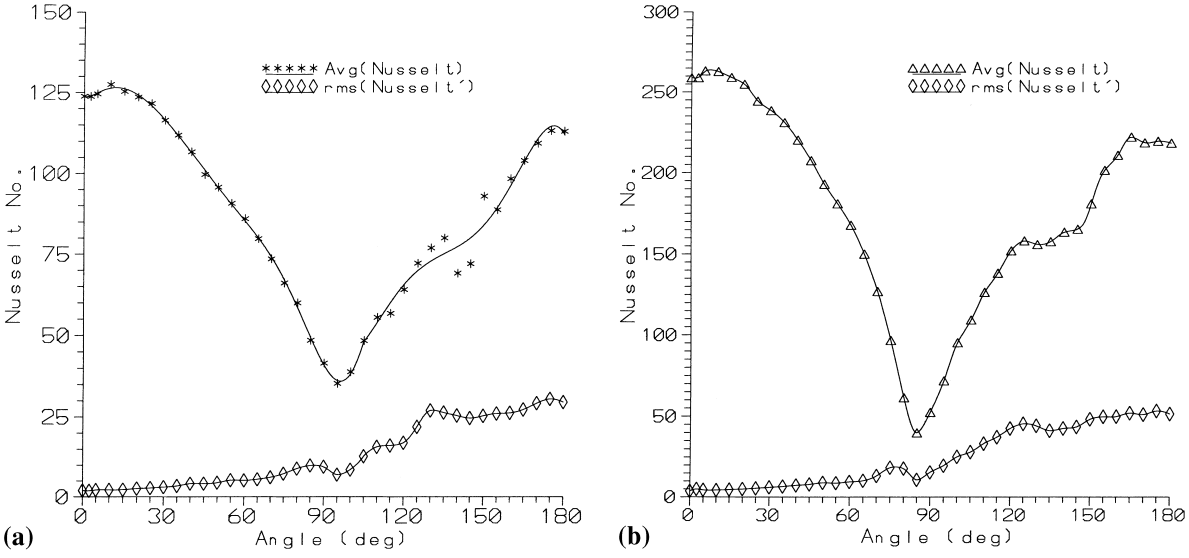

Fig. 7. Local Nusselt numbers at the second row: (a) $U = 5$ m/s; (b) $U = 15$ m/s.

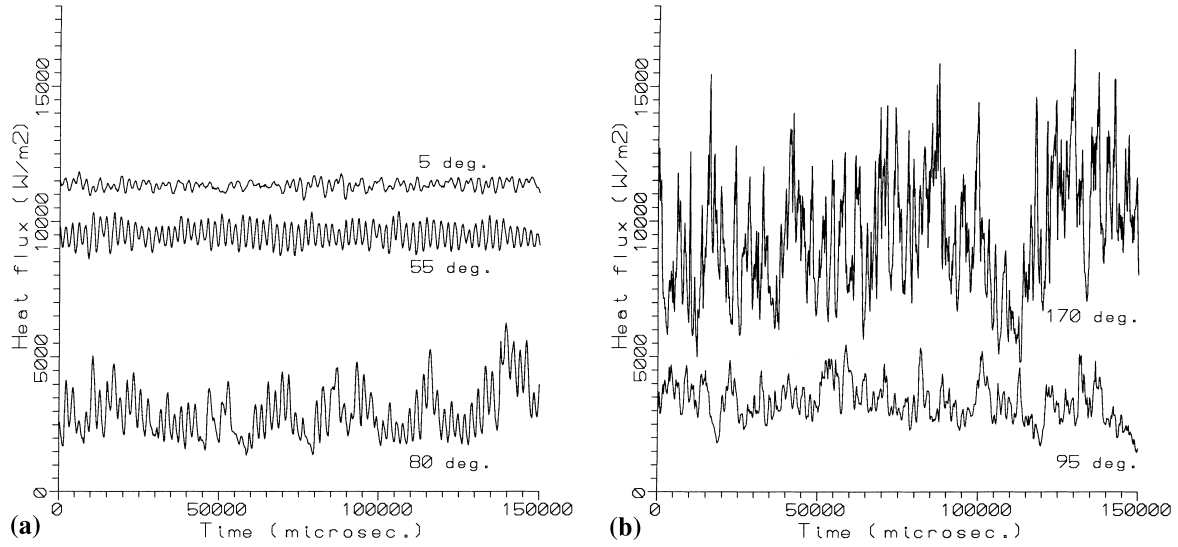

Fig. 8. Heat transfer time traces at the second row: $U = 15$ m/s: (a) positions preceding separation; (b) positions following separation.

Fig. 5 shows the velocity and surface heat flux auto spectra obtained from simultaneous measurements at the first row with the velocity of 15 m/s. The data were obtained at a position of 65° which is representative of positions preceding boundary layer separation or transition. It can be seen that both spectra contain frequency peaks at 325 and 515 Hz, associated with vortex shedding from the second and first rows, respectively. However, because the fluctuations in heat transfer are very small, the heat flux auto spectrum also shows peaks associated with mains noise.

The coherence level and phase difference obtained for the simultaneous measurements at the first row are shown in Fig. 6. It can be seen that high levels of coherence are obtained for the vortex shedding frequencies of 325 and 515 Hz and that an additional peak is present at 190 Hz. This frequency is equal to the difference between the frequencies for first and second row shedding and may be related to a non-linear interaction between the vortex shedding frequencies, as discussed later. In the auto spectra of Fig. 5, this interaction frequency is swamped by random fluctuations and mains noise. From Fig. 6(b), it can be seen that the phase difference is small up to a frequency of approximately 600 Hz. At higher frequencies, the phase becomes random. The significance of this is discussed later.

3.2. Second row

Fig. 7 shows the time-averaged local Nusselt numbers for a cylinder in the second row, together with the rms values of the unsteady heat transfer. At 5 m/s, it can be seen that the minimum Nusselt number position has moved forward to 95° and that the Nusselt numbers have risen generally, as compared to those recorded at the first row. A similar movement forward of the minimum Nusselt number position at the second row in a staggered array was reported by Baughn et al. (1986). The increase in fluid velocity to 15 m/s leads to a still earlier mini-

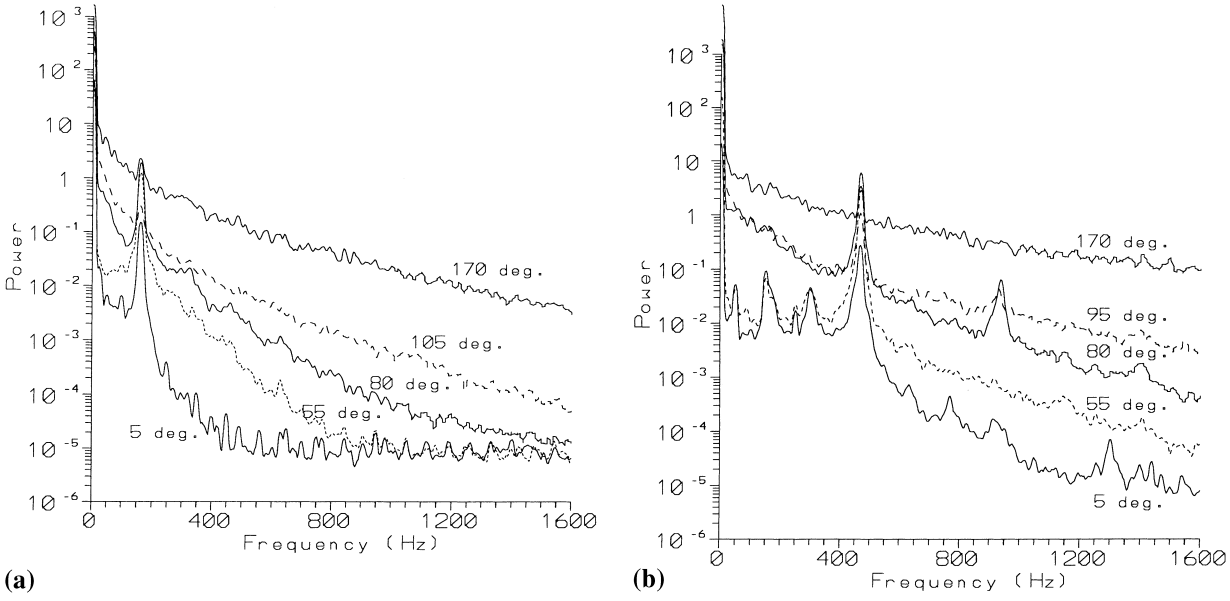

Fig. 9. Heat transfer auto spectra at the second row: (a) $U = 5$ m/s; (b) $U = 15$ m/s.

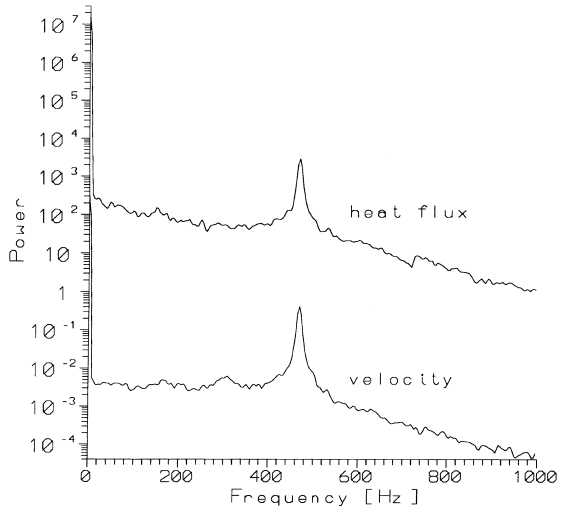

Fig. 10. Simultaneous auto spectra at the second row, 65°.

mum Nusselt number position and higher heat transfer levels generally. From the rms data, an increase in heat transfer fluctuations is evident over the tube front although these are still very small compared with the large fluctuations measured in the wake. The increase in heat transfer fluctuations is most significant over the tube sides and is linked to the increase in velocity fluctuations from vortex shedding at the first row.

In Fig. 8, time traces of the heat flux signal at the second row are shown for the velocity of 15 m/s. For the positions preceding boundary layer separation, a strong periodicity can be seen. Following separation, there is a higher content of random fluctuations with less evidence of periodicity. This is consistent with the results for the first row. The heat transfer spectra at the second row are shown in Fig. 9. At 5 m/s, it is only possible to clearly identify the peak from first row vortex shedding (160 Hz). This is because random fluctuations in the low frequency range associated with second row shedding swamp the individual peaks. At 15 m/s, for positions in advance of separation, several frequency peaks can be seen with the dominant peak at 470 Hz corresponding to vortex shedding from the first row. The peak at 300 Hz corresponds to second row vortex shedding and the peak at 170 Hz represents an interaction between the two vortex shedding processes. At 80°, there is an additional peak at twice the frequency associated with first row vortex shedding. Following separation, it is clear that the level of high frequency fluctuations is increased dramatically.

Simultaneous velocity and heat flux auto spectra at the second row are given in Fig. 10 for the velocity of 15 m/s and an angular position of 65°. In both cases, the dominant peak in the spectrum relates to the vortex shedding frequency for the first row. The coherence and phase difference between the velocity and the heat flux signals are shown in Fig. 11. It can be seen that a high coherence value is obtained for this vortex shedding frequency. When compared to the coherence obtained for the first row, it is also evident that the peak in coherence is more broad band in nature. In contrast to the phase plot for the first row, it can be seen that the phase shows a steep increase with increasing frequency.

3.3. Third row

The local variation in time-averaged Nusselt number at the third row differs significantly for the velocities of 5 and 15 m/s, as shown in Fig. 12. This is because the higher velocity, coupled with the high turbulence levels at the third row, triggers transition to turbulence within the boundary layer. In this case, the first heat transfer minimum corresponds to transition to turbulence within the boundary layer and the second to separation of the turbulent boundary layer. The presence of two heat transfer minima at the third row of a staggered array has been reported also by Zukauskas (1972) and Baughn et al. (1986). At an upstream velocity of 5 m/s the boundary layer remains laminar so that only one heat transfer minimum is observed. For both velocities, the mean Nusselt numbers at the third row differ by around 2% from the values calculated from the correlation of Zukauskas (1972) for the inner rows of a staggered array. From Fig. 12, it can also be seen that the fluctuations in heat transfer over the tube front have increased dramatically with respect to those measured at the earlier rows; there is now a near uniform level of fluctuations over the entire circumference.

Sample time traces of the heat flux signal for angular positions before and after boundary layer transition and following separation are shown in Fig. 13(a)–(c) respectively for the

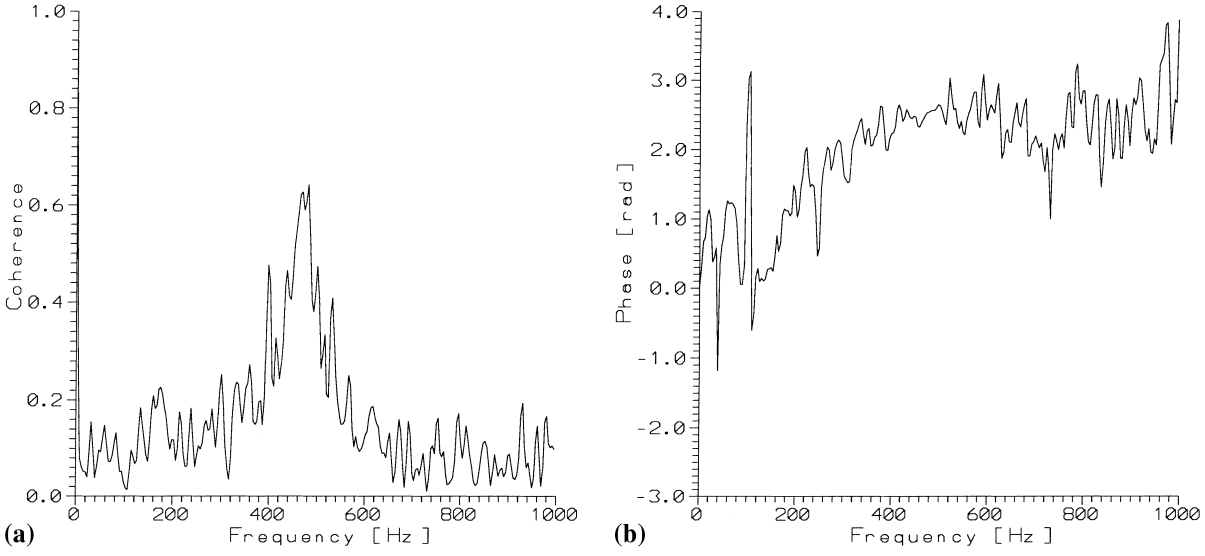

Fig. 11. Coherence and phase difference of LDA and heat flux signals at the second row: (a) coherence; (b) phase difference.

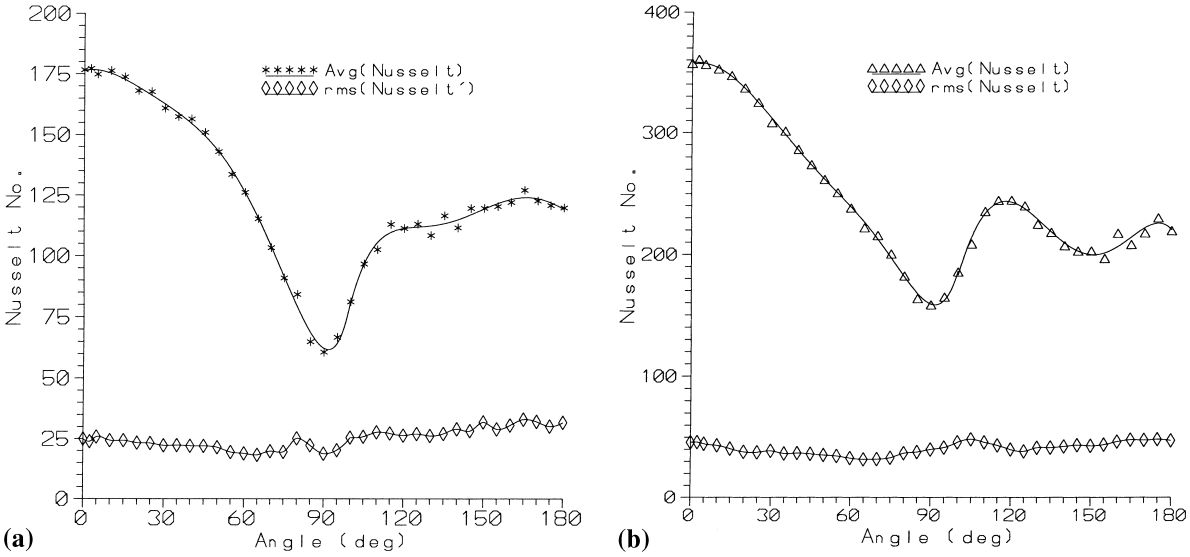

Fig. 12. Local Nusselt numbers at the third row: (a) $U = 5$ m/s; (b) $U = 15$ m/s.

velocity of 15 m/s. Despite the differences in the flow regime corresponding to the three sets of data shown, it is clear that the heat transfer fluctuations do not vary significantly with angular position. The heat transfer auto spectra for the cylinder in the third row are shown in Fig. 14. Because of the very high level of random fluctuations, frequency peaks associated with vortex shedding cannot be detected at the lower velocity. At the velocity of 15 m/s, very small peaks corresponding to one or other of the vortex shedding frequencies can be picked up at most of the angular positions shown. However, the main feature of these plots is the increase in the level of high frequency fluctuations together with the similarity in shape of the auto spectra at different angular positions. This is considered to be a consequence of the degeneration of coherent, large scale vortices into a generally high level of random fluid motion and turbulence at the third row.

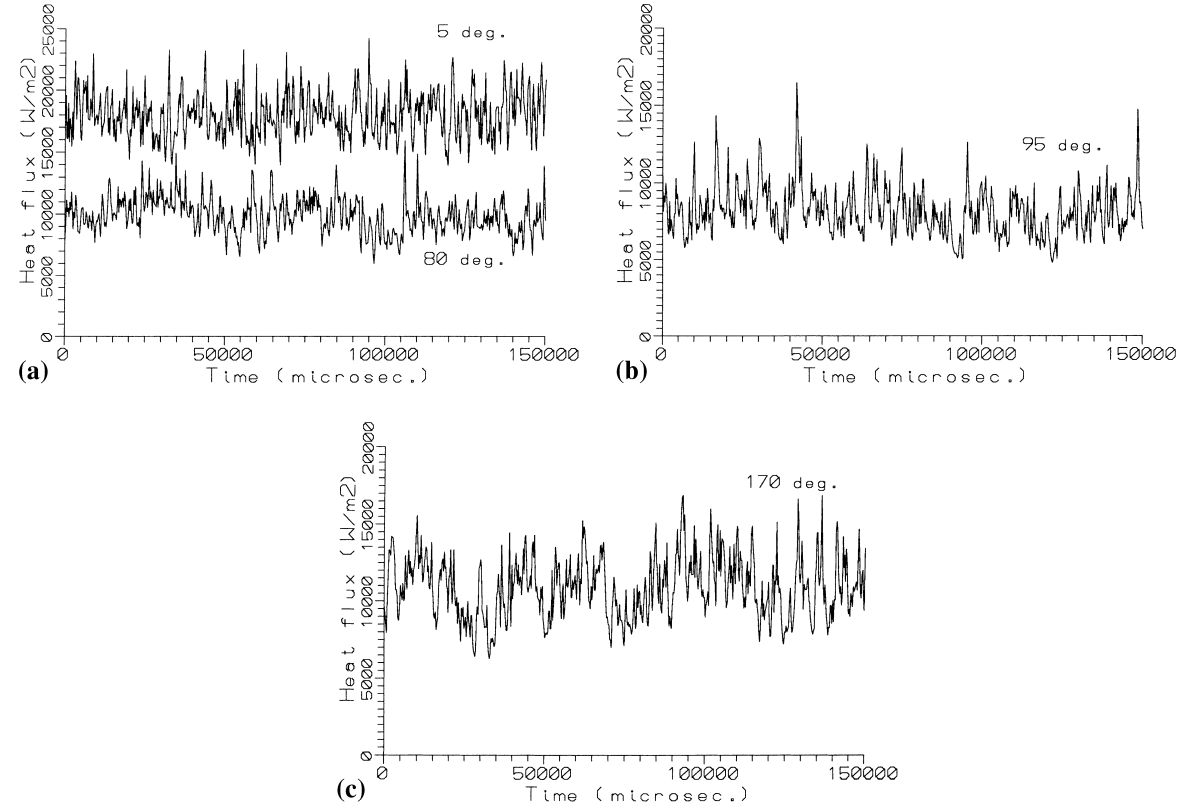

Fig. 13. Heat transfer time traces at the third row: $U = 15$ m/s: (a) positions preceding boundary layer transition; (b) position following transition; (c) positions following turbulent boundary layer separation.

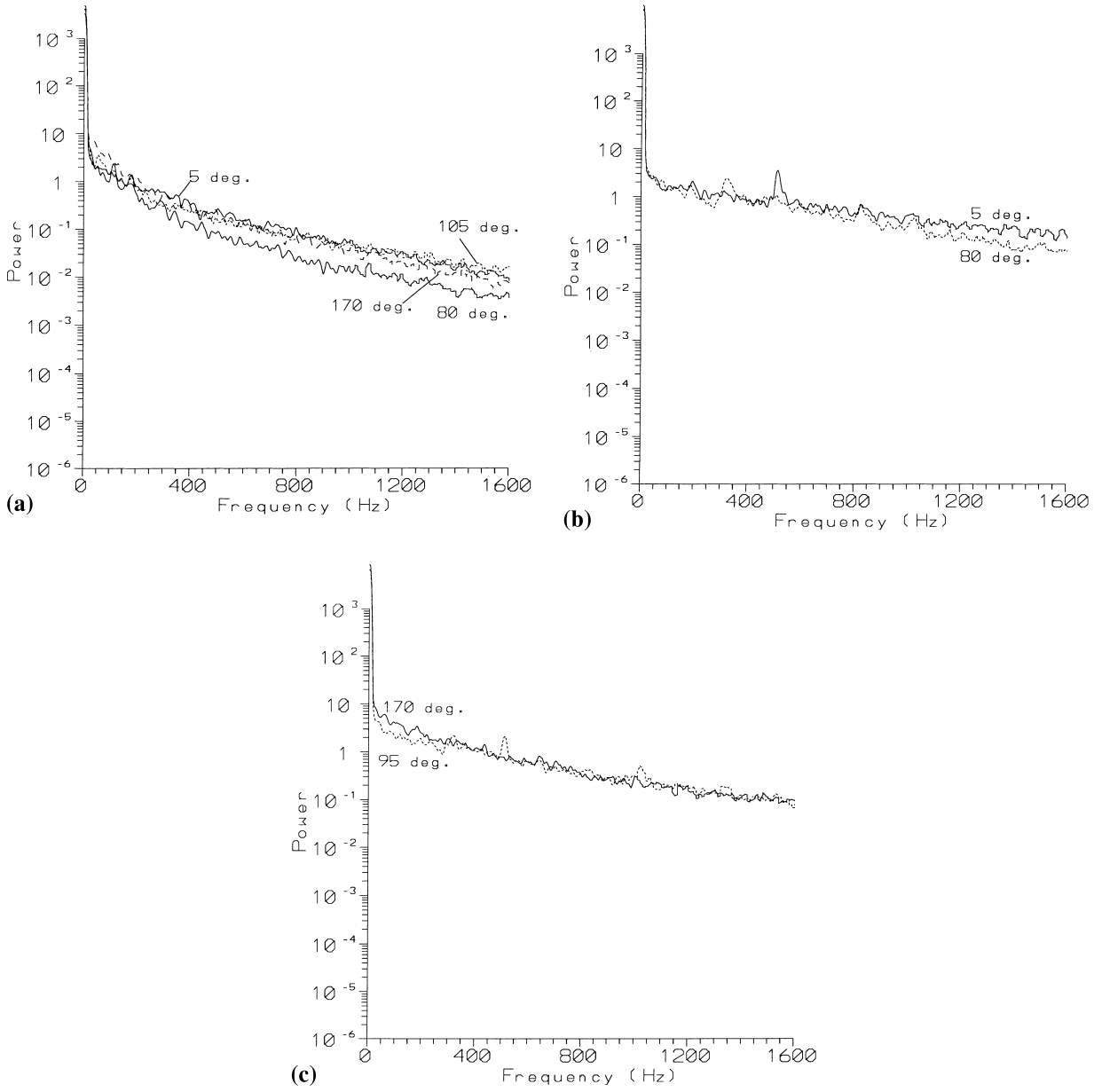

Fig. 14. Heat transfer auto spectra at the third row: (a) $U=5$ m/s; (b) $U=15$ m/s, before boundary layer transition; (c) $U=5$ m/s, after transition (95°) and separation (170°).

Fig. 15 shows the auto spectra for velocity and heat flux at 65° for a cylinder located in the third row. The frequencies associated with vortex shedding within the array can just be distinguished in the velocity spectrum, but are indistinguishable in the spectrum for the surface heat flux. This lack of periodicity in both the velocity and the heat transfer rate is in keeping with the degeneration and breaking down of the vortices shed, as the flow moves through the array. Fig. 16 shows the coherence and phase difference for this case. The level of coherence shown is lower than that obtained for both the first and the second rows. Instead, a very broad band and low level coherence is obtained, with a slightly raised level in the range around the vortex shedding frequencies. In addition, small peaks can be seen at the shedding frequencies, and at the interaction frequency. From Fig. 16(b), it can be seen that the phase rises steeply with increasing frequency, similar to the trend at the second row.

4. Discussion

One apparent anomaly in the results presented here concerns small differences in the frequencies associated with vortex shedding from the first and second rows, when detected at different tube locations. This is linked to subtle differences in the array geometry when testing at the first, second and third rows, as shown in Fig. 1 and arises from practical considerations concerning access to instrumentation. As a consequence of this, the gap velocity in the first row is lower when the geometry for testing in the second row of the array is used (configuration B). Thus, the vortex shedding frequency related to the first row, when testing in the second row, is 470 Hz as opposed to 515 Hz. The Strouhal numbers obtained from the correlation of Zukauskas and Katinas (1980) for first row shedding and from Weaver et al. (1987) for second row shedding are shown in Table 1 and those derived from measured frequencies

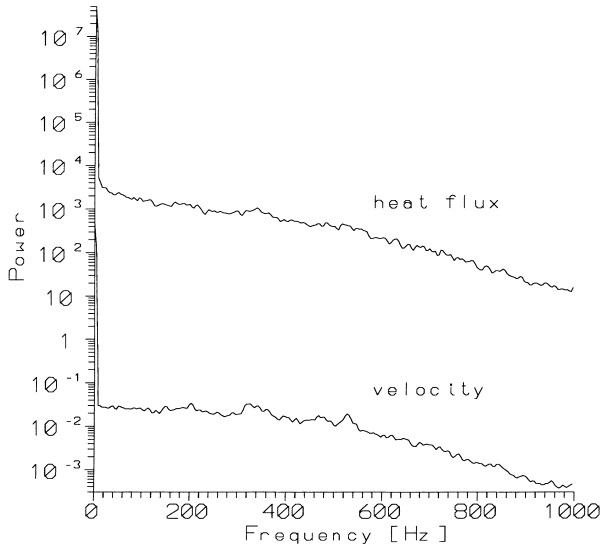

Fig. 15. Simultaneous auto spectra at the third row, 65°.

are shown in Table 2. The agreement between measured and expected Strouhal numbers for both rows is excellent for configuration A and for configuration B there is a maximum difference of some 15%. Clearly, the difference in vortex shedding frequencies between the two configurations is a consequence of both gap velocity and the flow asymmetry resulting from rows with only two or three tubes.

In addition to the dominant frequencies associated with vortex shedding from the first and second rows, a third peak equal to the difference between the two vortex shedding frequencies was detected for the higher velocity. This can be seen from Fig. 9. The existence of a frequency peak exactly equal to the difference between the other dominant peaks has been reported by Oengoren and Ziada (1995) for a staggered tube array with the same pitch to diameter ratio of 2. This peak was found to be most significant behind the second row and was attributed to a non-linear interaction between the two vortex shedding frequencies. A similar non-linear interaction between dominant frequencies in a separated shear layer was reported by Miksad (1973).

The coherence between surface heat flux and local fluid velocity signifies the extent to which the fluctuations in heat transfer originate in local velocity fluctuations. Comparison of the coherence plots from Figs. 6, 11 and 16 shows a progressive change from a very narrow peak of high coherence at the vortex shedding frequency at the first row through to a very broad band and low level of coherence at the third row. There are two factors which contribute to this change. Firstly, the local flow velocities vary as the fluid moves through the array, leading to a variation in the vortex shedding frequencies. Secondly, the coherent vortices shed from tubes in the first and second rows degenerate as the fluid moves through the array. At the third row, the very broad band low level coherence can be attributed to this breaking up of the vortices with progression through the array.

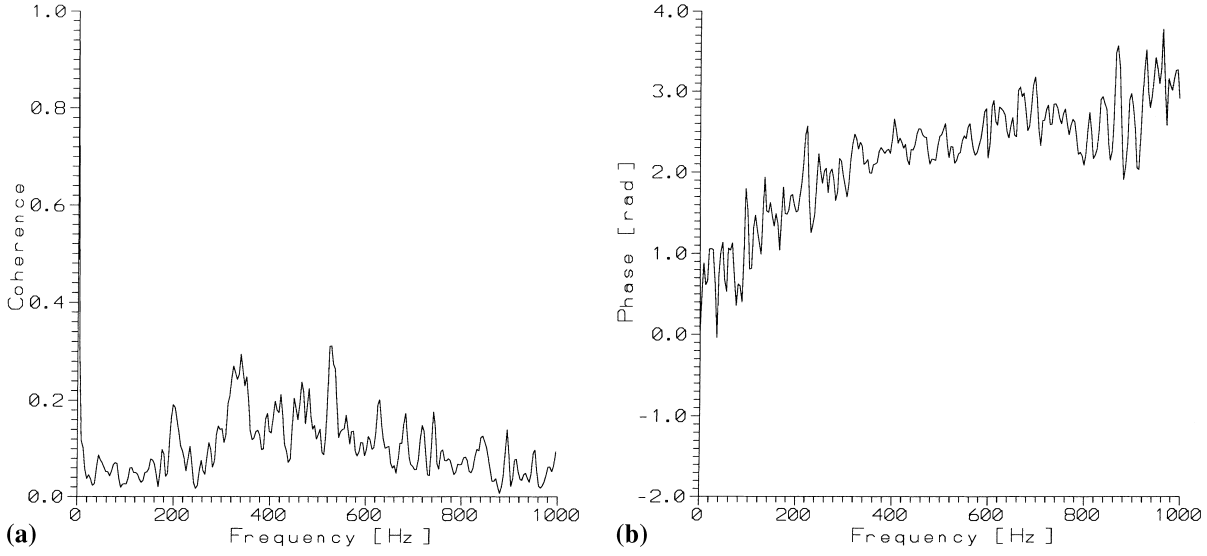

Fig. 16. Coherence and phase difference of LDA and heat flux signals at the third row: (a) coherence; (b) phase difference.

Table 2
Measured vortex shedding frequencies at first and second rows, when testing with configurations A and B

Velocity (m/s)	First row				Second row			
	Frequency (Hz)		Strouhal number		Frequency (Hz)		Strouhal number	
	A	B	A	B	A	B	A	B
5	170	160	0.85	0.8	110	–	0.55	–
15	515	470	0.85	0.78	330	300	0.55	0.5

The phase difference between the surface heat flux and the local velocity also indicates the influence of the flow field on the fluctuations in heat transfer. From Fig. 9(b), it can be seen that at the first row the phase difference is very small up to a frequency of approximately 600 Hz. Beyond this, the phase becomes random. This phase plot is very similar to that obtained by Scholten (1996) for a single cylinder in cross flow with the same upstream flow conditions as the present study. The near zero phase difference between surface heat flux and local fluid velocity is explained by the fact that a growing vortex imposes a larger resistance to the flow on its own side of the cylinder, thus reducing the flow velocity on that side. At the opposite side, the local flow velocity increases in order to maintain a constant mean flow. The implication of this is that the entire flow field pulsates, even in front of the cylinder, as a consequence of the formation and shedding of vortices at the back. Confirmation that the heat transfer fluctuations originate in a pulsating flow field for the single cylinder was obtained by Scholten (1996) by examining the phase difference between the surface heat flux and velocity measured at a number of different locations on both sides of the cylinder. From the similarity between the single cylinder and first row phase plots, it is concluded that most of the heat transfer fluctuations at the front of the first row tube result from pulsation originating in downstream vortex generation and shedding.

At the second and third rows, Figs. 11(b) and 16(b) show that the phase difference rises steeply with increasing frequency. This is similar to the phase obtained for a single cylinder in a highly turbulent cross flow by Scholten (1996). In that case, it was concluded that most of the velocity fluctuations are due to the transport of small turbulent eddies within the main flow. The radial motion of these eddies has a significant influence on surface heat flux, but the low radial velocity results in a time delay between the measured velocity 1 mm from the surface and the surface heat transfer fluctuations. This shows up in the steep slope of the phase difference. Beyond a frequency of around 600 Hz, the phase difference flattens out as a consequence of the zero phase difference from the higher content of step noise in this frequency range, Scholten (1996). This step noise is associated with resampling of the random time distribution of the data points.

For the single cylinder in a highly turbulent cross flow, Scholten (1996) compared the time delay between the fluctuations in measured heat transfer and velocity, estimated from the phase plot, with that estimated from the local fluid velocity and the distance between measurement points to show that the measured phase difference was consistent with the radial transport of small turbulent eddies as the origin of the surface heat transfer fluctuations. The similarity between the phase plots for that case and for the tube in the second and third rows suggests that the fluctuations in heat flux at these locations also result from the radial motion of small turbulent eddies rather than from pulsation of the flow field due to vorticity.

The fact that the dominant influence on heat transfer for the inner rows of a staggered array is the high turbulence generated by vortex shedding from the upstream tubes is a familiar result from studies of time-averaged heat transfer, Zukauskas (1972). However, the present study of simultaneous velocity and heat transfer fluctuations has identified that the large scale coherent vortices have degenerated into small scale turbulence by the third row. This has implications for the design of tubular heat exchangers as it suggests that results obtained from tests conducted on small three row arrays may be broadly applicable to the larger tube arrays more likely to be used in practice.

5. Conclusions

An experimental investigation of fluctuating heat transfer and velocity in a three row staggered tube array has been conducted. Tests were carried out for two Reynolds numbers and three tube positions and measurements were obtained at a number of angular positions on the tube surface. From the results obtained, the following conclusions can be drawn:

1. The level of fluctuations in surface heat flux is low at the front of a cylinder in the first row. The small measured fluctuations result from a locally pulsating flow field created by vortex formation and shedding within the array. For the back of a first row cylinder, the level of fluctuations is high.
2. For a second row cylinder, the fluctuations at the front of the cylinder are higher, and the level of fluctuations increases when the angular location of the heat transfer measurements lies more in the wake of the cylinders of the first row. From the phase difference obtained from simultaneous measurements, it can be concluded that the fluctuations in heat transfer lag the fluctuations in velocity, indicating that the radial transport of turbulent eddies is the dominant influence on the heat transfer fluctuations.
3. When a third row cylinder is considered, the level of the fluctuations in surface heat flux at the front of the cylinder is seen to be similar to the level obtained at the back. This high level of fluctuations is a result of a highly turbulent flow at this location, created by the vortex shedding from the first and second row tubes. When the velocity combined with the local turbulence level is high enough, transition of the boundary layer on the tube surface can take place. Simultaneous measurements indicate that the time variation in heat flux is governed by turbulent eddy transport rather than by vortex generation within the array.

Acknowledgements

The authors wish to thank Professor J.A. Fitzpatrick for his assistance with the spectral analysis procedures.

References

Achenbach, E., 1981. Total and local heat transfer and pressure drop of staggered and in-line tube bundles. In: Kakiac, S., Bergeles, A.E., Mayinger, F. (Eds.), Heat Exchangers-Thermal Hydraulic Fundamentals and Design, McGraw Hill, New York, pp. 85–96.

Balabani, S., Yianneskis, M., 1996. An experimental study of the mean flow and turbulence structure of cross-flow over tube bundles. Proc. I. Mech. E. J. Mech. Eng. Science 210, 317–331.

Baughn, J.W., Elderkin, M.J., McKillop, A.A., 1986. Heat transfer from a single cylinder, cylinders in tandem and cylinders in the entrance region of a tube bank with a uniform heat flux. ASME J. Heat Transfer 108, 386–391.

Beasley, D.E., Figliola, R.S., 1988. A generalised analysis of a local heat flux probe. J. Physics E 21, 316–322.

Bendat, J.S., Piersol, A.G., 1986. Random data analysis and measurement procedures. Wiley, New York.

Ching, C.Y., O'Brien, J.E., 1991. Unsteady heat flux in a cylinder stagnation region with high freestream turbulence. Fund. Exp. Meas. in Heat Transfer, ASME, HTD 179, 57–66.

Churchill, S.W., Bernstein, M., 1977. A correlating equation for forced convection from gases and liquids to a circular cylinder in cross flow. ASME J. Heat Transfer 99, 300–306.

George, G.H., 1993. Instantaneous local heat transfer coefficients and related frequency spectra for a horizontal cylinder in a high

temperature fluidised bed. Int. J. Heat Mass Transfer 36 (2), 337–345.

Katoh, Y., Miyamoto, M., Kohno, A., 1991. The study on unsteady heat transfer around a horizontal heated tube surface in a fluidised bed. Proceedings of the International Conference on Multiphase Flows, Tsukuba, vol. 1, pp. 317–320.

Meyer, K.E., Larsen, P.S., 1994. LDA study of turbulent flow in a staggered tube bundle. Seventh International Symposium on Applications of Laser Anemometry to Fluid Mechanics, Lisbon, pp. 39.4.1–39.4.7.

Miksad, R.W., 1973. Experiments on non-linear interaction of a free shear layer. J. Fluid Mechanics 59 (1), 1–21.

Oengeren, A., Ziada, S., 1995. Vortex shedding, acoustic resonance and turbulent buffering in normal triangular tube arrays. Proceedings of the Sixth International Conference on Flow Induced Vibration, London, pp. 295-313.

Rosicskowski, J., Hollworth, B., 1991. Local and instantaneous heat transfer from an isothermal cylinder in a cross flow. Fund. Exp. Meas. in Heat Transfer, ASME, HTD 179, 49–56.

Rottger, H.K., Renz, U., 1994. Measurements of instantaneous local heat transfer coefficients around a tube immersed in a high temperature fluidised bed. Proceedings of the Tenth International Heat Transfer Conference, Brighton, vol. 2, pp. 285–290.

Scholten, J.W., 1996. Fluctuating heat transfer of cylinders in cross flow. Ph.D. thesis, University of Dublin, Trinity College.

Scholten, J.W., Murray, D.B., 1995. Time resolved heat transfer measurements for a cylinder with boundary layer transition, Proceedings of the Fourth UK National Conference on Heat Transfer, Manchester, pp. 111–115.

Scholten, J.W., Murray, D.B., Fitzpatrick, J.A., 1996a. Simultaneous measurement of time resolved heat flux and velocity for a tube in cross flow. Proceedings of the Second European Thermal Sciences and 14th UIT National Heat Transfer Conference, Rome, vol. 2. pp. 1063–1069.

Scholten, J.W., Murray, D.B., Fitzpatrick, J.A., 1996b. Measurements of unsteady velocity and heat transfer for cylinders in cross flow. Proceedings of the Eight International Symposium on Applications of Laser Techniques to Fluid Mechanics, Lisbon, vol. II. pp. 33.1.1–33.1.7.

Simmons, S.G., Hager, J.M., Diller, T.E., 1990. Simultaneous measurements of time-resolved surface heat flux and freestream turbulence at a stagnation point. Proceedings of the Ninth International Heat Transfer Conference, Jerusalem, vol. 2. pp. 375–380.

Simon, L., Scholten, J.W., Fitzpatrick, J.A., 1995. Velocimetrie laser: Amelioration du traitment des donnees experimentales par interpolation d'ordre 1. Proc. Congres Francais de Mecanique, Strasbourg. pp. 321–324.

Weaver, D.S., Fitzpatrick, J.A., ElKashlan, M., 1987. Strouhal numbers for heat exchanger tube arrays in cross-flow. ASME J. Pressure Vessel Technology 109, 219–223.

Zukauskas, A., Katinas, V., 1980. Flow induced vibration in heat exchanger tube banks. In: Naudascher, E., Rockwell, D. (Eds.), Practical Experiences with Flow Induced Vibrations, Springer, Berlin, pp. 188–196.

Zukauskas, A., 1972. Heat transfer from tubes in cross flow. Advances in Heat Transfer 8, 93–160.